Effect of Current Density on Magnetic and Hardness Properties of Ni-Cu Alloy Coated on Al via Electrodeposition

by Cahaya Rosyidan FTKE

International Journal of Engineering

Effect of Current Density on Magnetic and Hardness Properties of Ni-Cu Alloy Coated on Al via Electrodeposition

C. Rosyidan[a,b], B. Kurniawan[*a], B. Soegijono[c], V. G. Vidia Putra[d], D. R. Munazat[a], F. B. Susetyo[e]

[a] Department of Physics, Universitas Indonesia, Depok, Indonesia
[b] Department of Petroleum, Universitas Trisakti, Jakarta, Indonesia
[c] Department of Geoscience, Universitas Indonesia, Depok, Indonesia
[d] Plasma and Nanomaterial Research Group, Politeknik STTT Bandung, Bandung, Indonesia
[e] Department of Mechanical Engineering, Universitas Negeri Jakarta, Jakarta, Indonesia

*A B S T R A C T*

Nickel (Ni)-rich single-phase nickel-copper (Ni-Cu) alloy coatings were produced on aluminum (Al) substrates by electrodeposition in stabilized citrate baths. Electrodeposition experiments were performed at four different current densities. Increasing the current density resulted in the metal deposition rate increasing faster than the hydrogen evolution rate; thus, the cathodic current efficiency increased. The crystal systems of the Ni-Cu alloys were face center cubic (fcc), with the (111) plane as the preferred crystal plane. Scanning electron microscopy with energy dispersive X-ray spectroscopy (SEM-EDS) measurements showed that the Ni content in the coating increased with increasing current density. The Ni-Cu 40 sample had the most Ni content and showed a homogeneous and compact morphology. It was found that the higher the concentration of Ni in the solution, the smaller the grain size. Measurements recorded with a vibrating sample magnetometer (VSM) showed that the Ni-Cu 40 sample provided magnetic saturation, with the highest value being 0.108 emu/g. The microhardness method produced 404 HV on the Ni-Cu 40 sample. In conclusion, higher current densities were associated with a higher Ni composition and increased thickness, which were responsible for the increases in the magnetic properties and hardness.

doi: 10.5829/ije.2024.37.02b.01

Graphical Abstract
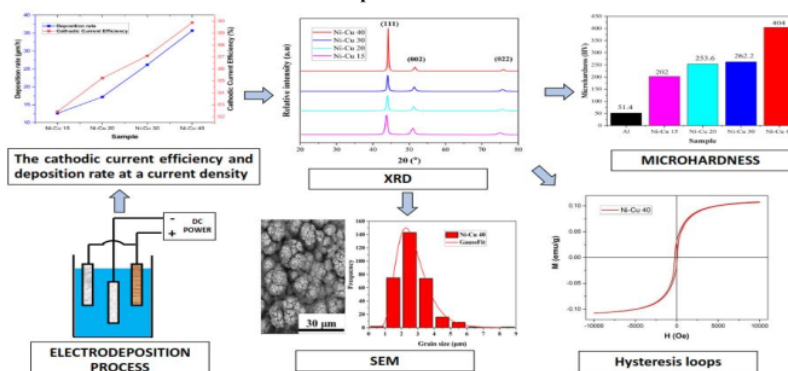
Corresponding author email: budhy.kurniawan@sci.ui.ac.id (B. Kurniawan)

NOMENCLATURE

C_e	Cathodic current efficiency	W_i	Initial weight of the substrate
σ	Lattice strain	W_f	Weight
W_s	Final weight of the substrate	I	Total current
W_m	Ratio of the final weight of the substrate	t	Deposition time
μ	Texture coefficient of the unique plane	F	Faraday's constant
$I(hkl)$	Measured intensity	f_{ni}	Nickel deposit weight ratio
m_{cu}	Copper's atomic weight	m_{ni}	Nickel's atomic weight

1. INTRODUCTION

Researchers widely study nickel (Ni) and copper (Cu) alloys as engineering materials due to their unique mechanical, magnetic, and anti-corrosion properties (1, 2). Ni-Cu alloys are known as monel in the industry and are typically comprised of 70 wt% Ni and 30 wt% Cu (3). These alloys have outstanding capabilities in acidic and alkaline environments (4). Ni-Cu alloys are single-phase alloys throughout their composition on the phase diagram, and these alloys formed because Ni and Cu are fully soluble in their solid and liquid states (5). Ni and Cu both have a face center cubic (fcc) crystal structure, and they have almost similar electronegativity and atomic radii (6, 7).

Given that conventional casting as a manufacturing method for monel results in substantial production costs and that Ni-Cu alloy coated on aluminum (Al) has potential as a replacement for monel as a bulk material (8), Al-based metals have received considerable attention (9, 10). They are lightweight and demonstrate high resistance to wear and corrosion and a high strength–stiffness combination (11).

Several techniques have been proposed to successfully modify the surface morphology and chemical composition, including sol-gel, chemical etching, chemical vapor deposition, thermal embossing, and electrodeposition (12, 13). The electrodeposition technique is a cost-effective, scalable, and easy-to-control process for coating Ni-Cu alloy (14). Specific methods have also been developed to determine the structure, morphology, and phase composition of the coated Ni-Cu alloys (15, 16). Goranova et al. (17) investigated how changing the concentration of Ni ions and the current density affected the structure and composition of Ni-Cu alloys formed by electrodeposition in alkaline citrate baths. Higher concentrations of Ni ions in the bath led to notably smoother deposits and enhanced current efficiency. However, producing a uniform Ni-Cu coating can be challenging due to the difference in reduction potential between Ni and Cu. The reduction potential of Ni atoms is -0.25 V vs. SHE, and that of Cu atoms is +0.34 V vs. SHE (18). As a result, controlling the concentrations of Ni and Cu is vital. Complexing agents must be added to narrow the potential difference between Ni and Cu. The most frequently used complexing agent is citrate due to its low toxicity, cost-effectiveness, and buffering characteristics (19).

The electrodeposition process affects the physical properties of the resultant Ni-Cu alloy, as does the current density. A high current density causes the crystal plane to be oriented in the (111) plane, the lattice size to be smaller, and the atomic distance to be less (20). The grain size becomes smaller when the current density is high, and the morphological shape resembles that of a cauliflower (21). As a result of a high current density, the coating will be thicker, and the composition of the Ni weight fraction will also be higher. The amount of Ni deposited on the substrate and the thickness of the coating both have an impact on the product's magnetic properties (22). In addition, a smaller grain size results in an increase in hardness (23). Karunakaran et al. (24) reported a hardness of 153 HV when the current density was 40 mA/cm^2, and Karunakaran and Pugazh (25) Vadivu reported a magnetic saturation value of 0.0004 emu/g at 40 mA/cm^2. Nevertheless, the researchers did not examine the impact of the coating electrodeposition factors, structure, and morphology on the magnetic and hardness properties.

The aims of this research were 1) to produce a Ni-rich Ni-Cu alloy coating on Al via electrodeposition and 2) to investigate the link between magnetic and hardness properties and the coating's microstructure and surface morphology. We varied the current density, and the process was conducted at room temperature. We examined the influence of various process variables on the cathodic current efficiency, structure, morphology, composition, grain size, and thickness of the produced coatings. Finally, the magnetic properties and hardness of the coatings were investigated.

2. MATERIAL AND METHODS

2. 1. Material and Electrodeposition Process
The chemical composition of the Al substrate (cathode) used was Fe = 1.63 wt%, Mg = 1.49 wt%, and Al = 96.88 wt%. The chemical composition of the Ni (anode) used was Al = 0.02 wt%, Ca = 0.04 wt%, Fe = 0.23 wt%, Y = 1.61 wt%, Zr = 0.04 wt%, Nb = 0.05 wt%, and Ni = 98.01 wt%. The chemical composition of the Cu (anode) used was P = 0.22 wt%, Cd = 0.684 wt%, Si = 0.137 wt%, and Cu = 98.959 wt%. The Al was cleaned from the oxide coating with sandpaper before deposition using DELTA D68H for 5 min. Ni-Cu electrodeposition was carried out using a SANFIX 305 E DC power supply. The samples produced using a current density of

15 mA/cm^2, 20 mA/cm^2, 30 mA/cm^2, and 40 mA/cm^2 were designated as Ni-Cu 15, Ni-Cu 20, Ni-Cu 30, and Ni-Cu 40, respectively. Table 1 summarized the bath composition and deposition parameters.

2. 2. Characterization The deposition rate was calculated using the previously reported method (26). The following formula, Equation 1, was used to calculate the efficiency of the cathodic current (27):

$$C_e = {W_m}/{W_f} \qquad (1)$$

W$_m$ and W$_f$ were calculated using Faraday's law, as shown in Equations 2 and 3.

$$W_m = W_s - W_i, \qquad (2)$$

$$W_f = \{(m_{ni}/2) * f_{ni} + (m_{cu}/2) * f_{cu}\} * I . \frac{t}{F}. \qquad (3)$$

The crystal structure of the Ni-Cu coating was determined using X-ray diffraction (XRD-PANanalytical Aeris Instrument Suit) (Cu-Kα radiation, λ = 0.15418 nm). XRD data were collected from 20° to 80° with a step size of 0.020°. The Materials Analysis Using Diffraction (MAUD) program was used to determine the crystal parameters of the sample after Rietveld refinement. The preferential crystallite orientation was determined from the texture coefficient μ, as shown in Equation 4 (28):

$$\mu = \frac{I(hkl)/I_0(hkl)}{(\frac{1}{N})\sum[I(hkl)/I_0(hkl)]}, \qquad (4)$$

Based on XRD results, the lattice strain σ was calculated using Equation (5) (29):

$$\sigma = \left(\frac{\beta}{4 \times \tan\theta}\right) \qquad (5)$$

SEM-EDS (Thermofisher Quanta 650 EDAX EDS Analyzer) with 1000× magnification was used to analyze the surface morphology of the Ni-Cu coatings. EDS was used to determine the chemical composition of the coatings, and the statistical distribution of grain sizes was calculated using ImageJ software. The cross sections of the coated samples were also examined to assess how the current density and CCE affected the

TABLE 1. Bath composition and deposition parameters

Bath composition and condition	Quantity
NiSO$_4$.6H$_2$O (Merck)	0.5 M
CuSO$_4$.5H$_2$O (Merck)	0.04 M
Na$_3$C$_6$H$_5$O$_7$ (Merck)	0.2 M
pH	4.2
Temperature	25 °C
Deposition time	1 h

coating thickness. Measurement of magnetic properties was conducted using a vibrating sample magnetometer (VSM, Oxford 1.2H). The hardness of the Ni-Cu coatings was measured using a MicroMct® 5100 Series Microindentation Hardness Tester. The ATM E384 standard was used for the tests, which were performed with a load of 100 g for 10 s at five places.

3. RESULTS AND DISCUSSION

3. 1. Cathodic Current Efficiency and Deposition Rate Figure 1 depicts the relationship between the average CCE and deposition rate in the citrate electrolyte bath. The CCE was found to be high, with a value of 82–89%. The basic concept of current efficiency can be understood as the fraction of total current used for metal plating (30). Apart from metal deposition, hydrogen evolution is the only other necessary process that must occur on the substrate surface. Ni and Cu precipitation are both antagonistic to the hydrogen evolution reaction. In this study, the metal deposition rate increased faster than the hydrogen evolution rate when the current density increased from 15 to 40 mA/cm^2; hence, the CCE increased. The highest CCE (89.96%) was associated with the Ni-Cu 40 sample, and the lowest CCE (82.55%) was associated with the Ni-Cu 15 sample. Basori et al. and Syamsuir et al. (31) found that the deposition rate and current efficiency are considered linear.

3. 2. Structural Properties Figure 2(a) depicts the XRD spectra of the Ni-Cu alloy samples produced at various current densities. According to the XRD analysis results, each Ni-Cu alloy sample consisted of a single phase with an fcc structure. The evolution of the lattice parameters of the Ni-rich (111) phase over the range of current densities is shown in Figure 2(b). The
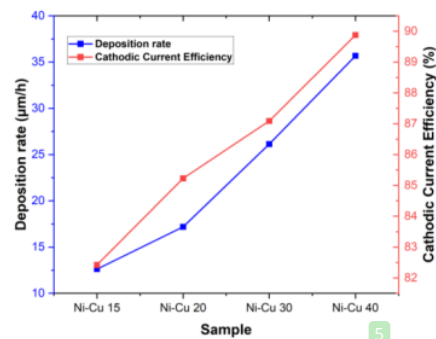

Figure 1. The cathodic current efficiency and deposition rate at a current density of 15, 20, 30, and 40 mA/cm^2
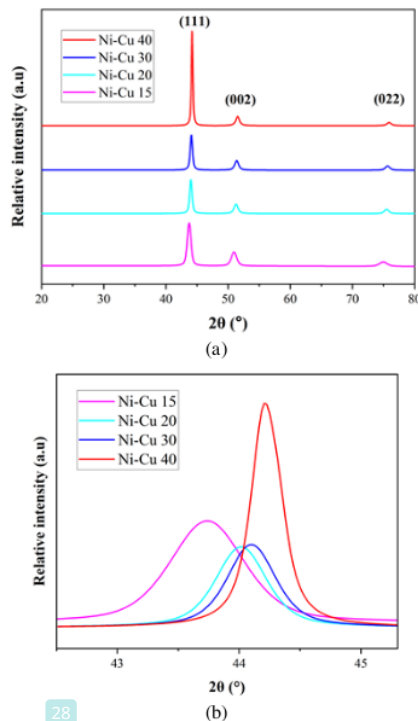
Figure 2. (a) X-ray diffraction spectra of Ni-Cu coatings electrodeposited at various current densities and (b) the extended view of the Ni-Cu (111) plane, showing peak shifts

peaks of each sample were found between the peaks of the fcc of 2θ = 43.3° for pure Cu and 2θ = 44.5° for pure Ni (32, 33). As the Ni content of the alloy coating increased, the diffraction angle also increased.

Crystal size calculation using MAUD resolved refinement was used to determine the size of the crystallites in the Ni-Cu alloys, and the results (Table 2) show that the crystallite size of the Ni-Cu coating ranged from approximately 24 to 50 nm. The crystallite size of a pure Ni layer is 60 nm, meaning that the Ni-Cu alloys had smaller crystallite sizes than a pure Ni layer. This result is also similar to that obtained by Li et al. (34). In contrast to the typical watt-Ni coating, we found that the presence of a sodium citrate complexing agent resulted in a finer crystallite size. This is consistent with the findings of Sarac and Baykul (35), who observed that Cu atoms affect grain refinement in Ni-Cu alloys. Cu atoms can restrain the surface diffusion of Ni atoms during the deposition process and inhibit the growth of crystallites.

The evolution of the crystallographic orientation of the Ni-Cu coatings produced with varying current

densities is shown in detail in Figure 3. It can be observed that a strong (111) fiber texture appeared in all the samples, while the (002) texture gradually decreased as the current density increased.

The μ values of different crystal planes are also used to evaluate the degree of crystallographic orientation (34). Moreover, the Ni-Cu coating electrodeposited at the current density of 40 mA/cm² was found to have a strong (111) texture.

The texture coefficient for every preference was calculated using Equation 4 to ascertain the preferred crystal orientation direction of each Ni-Cu alloy obtained at the various current densities, and the results are shown in Table 3 (32).

It seems that the texture coefficient was also dependent on the peak current, and the preferred orientation was the (111) plane. Li et al. (34) found that the higher the current density, the more dominant the (111) plane. The findings suggest that the (111) crystallographic orientation was preferable for all the Ni-Cu coatings electrodeposited at the tested current densities.

The lattice strain of the prepared coatings was determined using Equation 5, and Figure 4 illustrates the changes in the crystal size and lattice strain of the Ni-Cu coatings based on the current density applied in the plating bath.

The crystal size increased and the lattice strain decreased as the current density increased (36). This result aligns with that obtained by Devi et al. (33), who showed that the higher the current density, the more the
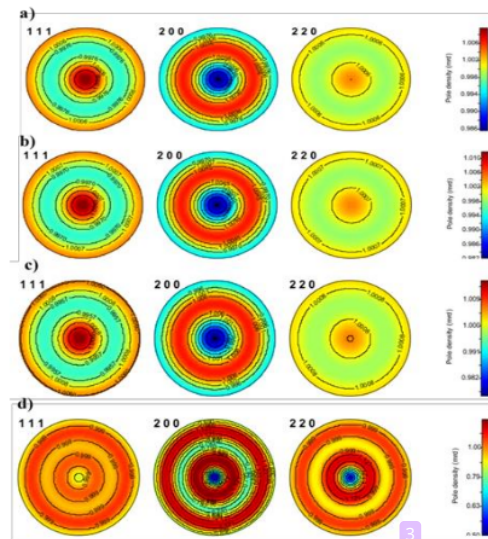

Figure 3. The simulated 2D pole figures for the (a) Ni-Cu 15, (b) Ni-Cu 20, (c) Ni-Cu 30, and (d) Ni-Cu 40 samples

TABLE 2. Parameters of the Ni-Cu alloys after Rietveld refinement using MAUD

Parameter	Sample			
	Ni-Cu 15	Ni-Cu 20	Ni-Cu 30	Ni-Cu 40
Crystal structure		Cubic fcc		
Space group		Fm-3m		
Lattice constant (Å) a = b = c	3.582	3.560	3.554	3.545
Volume (Å³)	45.975	45.152	44.905	44.557
d-spacing (Å)	1.791	1.780	1.695	1.691
Crystallite size (nm)	24.55	26.82	32.29	50.78
Rwp (100%)	3.640	4.484	5.394	5.139
GOF	1.94	1.72	2.06	2.03
Lattice strain	0.663	0.453	0.431	0.276

TABLE 3. Texture coefficient analysis of Ni-Cu deposits

Sample	μ (hkl)		
	[111]	[002]	[022]
Ni-Cu 15	1.12	0.86	0.77
Ni-Cu 20	1.17	0.74	0.81
Ni-Cu 30	1.18	0.74	0.78
Ni-Cu 40	1.48	0.34	0.32
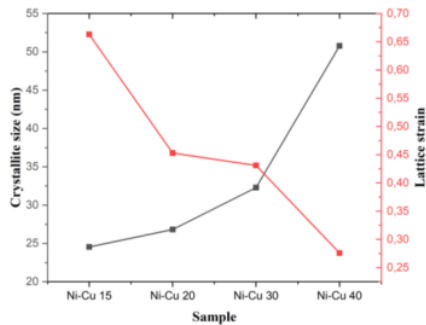
Figure 4. The lattice strain and crystallize size of the Ni-Cu alloys coated on Al at various current densities

crystal size increased. A possible reason for this is that the composition of Ni increases as the current density increases.

3. 3. Surface Morphology   EDS was used to determine the elemental composition of the Ni-Cu coatings, and the results are shown in Figure 5 and Table 4. Cu and Ni were the only elements present in the

deposits. The alloy composition was influenced by the current density: as the current density increased, the Cu content decreased. This phenomenon can be caused by the [Ni²⁺]/[Cu²⁺] ratio in the bath, which changes the composition of Ni and Cu. Goranova et al. discovered that as the Cu content of deposits decreased, so did the CCE (37). This phenomenon occurs because of the orderly deposition of Ni and Cu (38). In regular deposition, increasing the current density leads to an increased proportion of less noble metals in the deposited material (39). In our scenario, Ni is the less noble metal. As a result, when the current density was higher, the deposits were richer in Ni.

Another notable feature was that as the current density increased, the peak shifted to the right (i.e., to higher 2θ values). The change in the alloy composition may have also caused this peak shift. The Ni concentration increased as the current density increased (see Table 4). Because Ni and Cu combine to produce a single-phase alloy, the diffraction peak shifted toward that of pure Ni as the Ni percentage increased. This finding is similar to the observations of Goranova et al. (17), who found that the fcc reflection for Ni-rich Ni-Cu alloy deposits shifted to the right as the Ni concentration increased. Indeed, it is logical to expect the Ni-Cu alloy peak to shift as the Ni content increase.
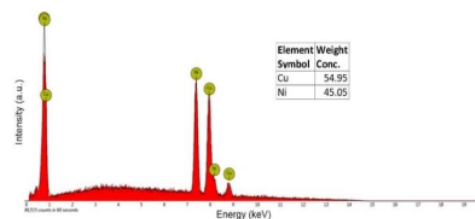

Figure 5. Eds graph of the Ni-Cu 15

TABLE 4. The chemical composition of Ni-Cu coatings on the Al substrate prepared at different current densities

Sample	Cu, wt%	Ni, wt%
Ni-Cu 15	54.95	45.05
Ni-Cu 20	39.83	60.17
Ni-Cu 30	29.80	70.20
Ni-Cu 40	19.64	80.36

The surface morphological structure and the cross section of the coated samples were observed using SEM. Figure 6 shows SEM micrographs of the four samples' surface morphological structures. The deposits developed a fine-grained and compact spherical shape when lower deposition current densities were applied (Figure 5(a)). Deo et al. (27) and Goranova et al. (37) also observed this morphology at low current densities. The shape changed to a coarser cauliflower form when higher current densities were applied (Figure 6(d)). A diffusion-limited deposition mechanism in which a multigeneration spherical diffusion layer creates a cauliflower shape is likely to produce this type of morphology (40). As the current density increased, the cauliflower-like protrusions became more spaced and separated, creating gaps. The Ni-Cu 40 sample, produced with the highest current density, was found to have the largest gaps between the cauliflower-like bulges.

The increased nucleation rate can explain the observed decrease in grain size with increasing current density (41, 42). Ni-Cu ion flow to the cathode is faster at higher current densities. Further investigation is
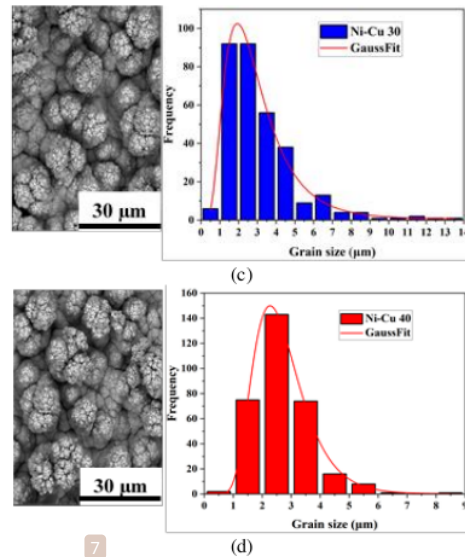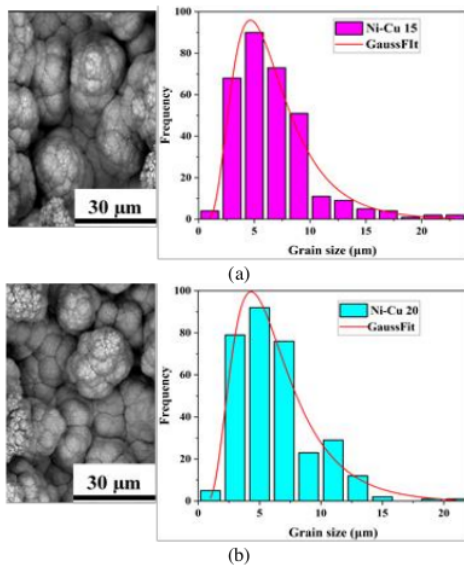

(a)

(b)

(c)

(d)

Figure 6. Surface SEM images of the deposited Ni-Cu alloy coatings and plots showing the statistical distribution of the grain size

needed to determine the exact relationship between the current density and the grain size of the coating. In the Ni-Cu 15, Ni-Cu 20, Ni-Cu 30, and Ni-Cu 40 samples, the peak that corresponded to the (111) plane shifted toward the right (see Figure 2b). The reduction in d-spacing is ascribed to residual stress induced at a higher deposition rate (43). The statistical results of the grain size distribution presented in Figure 6 indicate that the grain size ranged from 4.63 to 1.94 μm. The decrease in grain size with the increase in current density is evident in the data shown in Table 5.

Figure 7 depicts the relationship between the deposited alloy composition and the applied current density. EDS was used to determine the composition.

Figure 8 (a–d) displays SEM cross-section images of the produced Ni-Cu coatings. The absence of cracks between the substrate and coating demonstrates that appropriate adhesion occurred between the two entities (44). The thickness of the electrodeposited Ni-Cu coating was also measured for each sample (27), and the

TABLE 5. Average grain size found in each sample

Sample	Average grain size (μm)
Ni-Cu 15	4.63 ± 0.269
Ni-Cu 20	4.38 ± 0.365
Ni-Cu 30	2.28 ± 0.068
Ni-Cu 40	1.94 ± 0.032

following results were recorded: Ni-Cu 15 = 32 μm, Ni-Cu 20 = 42 μm, Ni-Cu 30 = 49 μm, and Ni-Cu 40 = 50 μm. The effect of the current density on the thickness of the Ni-Cu coating is depicted in Figure 8; the thickness increased as the current density increased (19). Hence, a higher current density results in more mass and a thicker coating. The findings presented in Figure 1 show that as the current density increased, so too did the CCE.

According to Faraday's law, when the deposition time remains constant for all samples, coatings formed at lower current densities will be thinner than those produced at higher current densities. A thinner covering may lead to severe interference from the Al substrate. The cathodic current density also affects the coating, as Deo et al. (27) discovered that increasing the current density improves the thickness of the film due to an increase in the CCE.

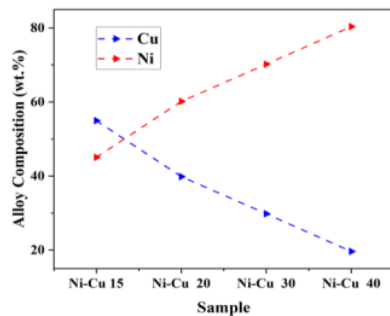**3. 4. Magnetic Properties**   Figure 9 depicts the magnetic characteristics and fluctuations in the current density magnetization measured with a VSM at room temperature (45). The results of the VSM analysis demonstrate that the coatings in the Ni-Cu 15, Ni-Cu 20, Ni-Cu 30, and Ni-Cu 40 samples displayed ferromagnetic activity. The low ferromagnetic activity of the $Cu_{54.95}Ni_{45.05}$ alloy film of Ni-Cu 15 could be attributed to Ni diffusion in the Cu matrix, as Cu is a diamagnetic metal and Ni is a ferromagnetic metal (46). The ferromagnetic properties of the Ni-Cu films of Ni-Cu 20, Ni-Cu 30, and Ni-Cu 40 increased with the Ni content of the alloy coatings.

Figure 7. The dependence of the deposited alloy's composition (shown as wt% of the single electrolytes) on current density
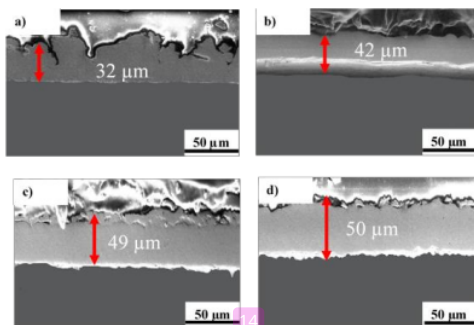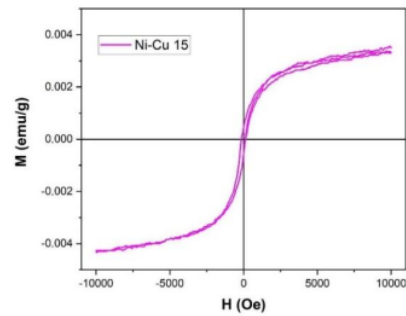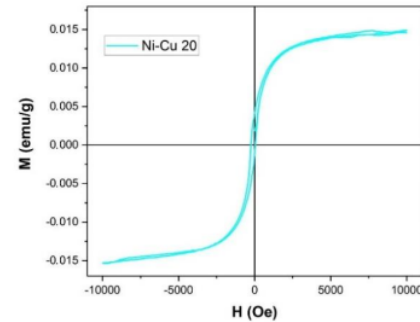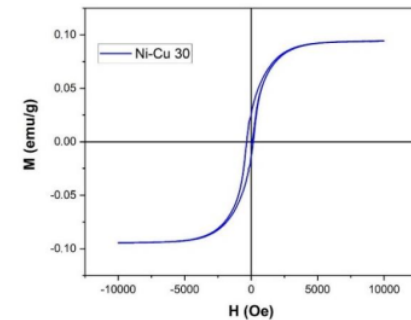

Figure 8. SEM cross-section images of the Ni-Cu coating on Al in the (a) Ni-Cu 15, (b) Ni-Cu 20, (c) Ni-Cu 30, and (d) Ni-Cu 40 samples

(a)

(b)

(c)
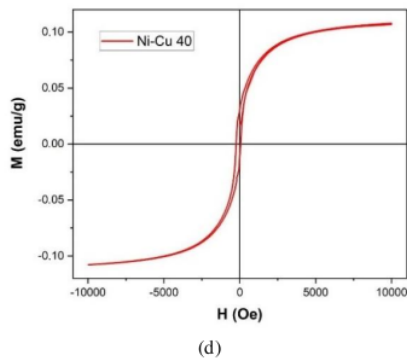
(d)

Figure 9. Hysteresis loops of multilayers generated at different current densities

Figure 10. The microhardness of the electrodeposited Ni-Cu samples produced with different current densities

As the Ni content of the Ni-Cu alloy coatings increased, so did the saturation magnetization (see Table 6). Wang et al. (43) reported that saturation magnetization depends on the Ni content of Ni-Cu alloy coatings. In addition, Awasthi (22) reported that magnetization is enhanced by increasing the coating thickness. A possible reason for this enhanced magnetization is the magnetic disorder caused by the coating. It has been shown that the trend in saturation magnetization enhancement is associated with the coating level (47). Demidenko et al. (48) found that monel has paramagnetic properties at room temperature, while the Ni-Cu alloys in this study had ferromagnetic properties. Here, we have improved upon the results of previous studies in which phosphorus (P) and tungsten (W) were added (25). In this study, the Ni-Cu 40 sample exhibited the strongest magnetic properties.

3. 5. Hardness   Figure 10 depicts the dependence of the microhardness of the Ni-Cu coatings on the current density in the plating bath. From the data presented in Figure 10, it is clear that the coating of the Ni-Cu 40 sample had the highest microhardness value (404 HV). In general, the microhardness increased with the current density and was attributed to the grain size and thickness of the coatings (42). Pingale et al. (19) found that hardness increased with the thickness of the coating. The

coating thickness could influence the hardness of Ni-Cu films (26).

The results indicate that alloys with a greater Ni content are mechanically harder. The overall dependence of hardness and microhardness on the percentage of Ni is shown in Figure 11, and the data indicate that microhardness increases as the percentage of Ni increase. This result is similar to Marenych's (49) finding that the hardness value is highest with the highest Ni composition.

Moreover, the hardness reported in previous studies that resulted from electrodeposition of Ni-Cu on Al in the presence of P was lower than that recorded in the present study (24). This is due to the smaller grain size that resulted from applying a different current density. In addition, the increase in microhardness reported here is related to the role that Ni atoms play in grain refinement (31). Ramkumar et al. (50) reported a monel hardness value of 165 HV, which is lower than the peak hardness value recorded in the current study.

TABLE 6. The results of the magnetic analysis of the Ni-Cu/Al samples

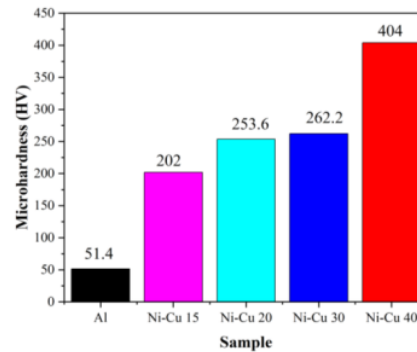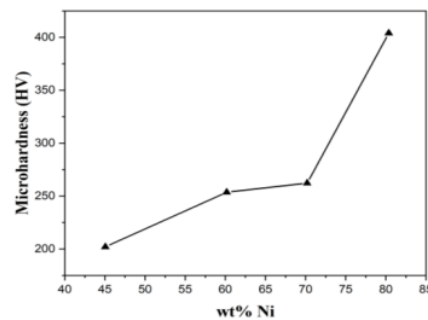| Sample	Hc (Oe)	Mr (emu/g)	Ms (emu/g)
Ni-Cu 15	143.829	0.00047	0.003
Ni-Cu 20	140.081	0.004	0.015
Ni-Cu 30	256.215	0.025	0.094
Ni-Cu 40	144.023	0.032	0.108

Figure 11. The relationship found between wt% Ni and microhardness, based on the data obtained from the four experimental samples

4. CONCLUSION

In this study, Ni-Cu alloys were electrodeposited onto Al substrates using citrate baths. The effects of adding a citrate solution on the properties of the deposited coatings were studied, and the results illustrate that single-phase Ni-Cu alloy layers were produced on the Al surface at all current densities. The CCE increased as the current density increased. The coatings formed at lower current densities showed a more compact and spherical morphology, while those formed at higher current densities showed a less uniform structure with a cauliflower-like morphology. Both the surface morphology and composition of the coating showed a strong dependence on the current density. The Ni-Cu alloy coating deposited at a low current density had a layer thickness of 32 μm, while the coating deposited at a high current density had a thickness of 50 μm. The saturation magnetization of the coating increased with the Ni content in the Ni-Cu alloy and with the coating thickness. The hardness increased with the coating thickness, grain size, and Ni composition in the solution. The hardness of the produced Ni-Cu alloy coatings was found to be greater than that of monel.

5. ACKNOWLEDGMENTS

6. REFERENCES

1. Chen Z, Wang C, Tang C, Lek YZ, Kandukuri SY, Du H, et al. Microstructure and mechanical properties of a Monel K-500 alloy fabricated by directed energy deposition. Materials Science and Engineering: A. 2022;857:144113. https://doi.org/10.1016/j.msea.2022.144113

2. Kukliński M, Bartkowska, A., and Przestacki, D. . Microstructure and selected properties of Monel 400 alloy after laser heat treatment and laser boriding using diode laser. International Journal of Advanced Manufacturing Technology. 2018;98(9-12): 3005–17. https://doi.org/10.1007/s00170-018-2343-9

3. Mohagheghpour E, Larijani M, Rajabi M, Gholamipour R. Effect of Silver Clusters Deposition on Wettability and Optical Properties of Diamond-like Carbon Films. International Journal of Engineering, Transactions C: Aspects, . 2021;34(3):706-13. https://doi.org/10.5829/ije.2021.34.03c.15

4. Nady H, Negem M. Ni–Cu nano-crystalline alloys for efficient electrochemical hydrogen production in acid water. RSC advances. 2016;6(56):51111-9. https://doi.org/10.1039/c6ra08348j

5. Negem M, Nady H. Electroplated Ni-Cu nanocrystalline alloys and their electrocatalytic activity for hydrogen generation using alkaline solutions. international journal of hydrogen energy. 2017;42(47):28386-96. https://doi.org/10.1016/j.ijhydene.2017.09.147

6. Guisbiers G, Khanal S, Ruiz-Zepeda F, De La Puente JR, José-Yacaman M. Cu–Ni nano-alloy: mixed, core–shell or Janus nano-particle? Nanoscale. 2014;6(24):14630-5. https://doi.org/10.1039/c4nr05739b

7. Mae Y. What the Darken–Gurry plot means about the solubility of elements in metals. Metallurgical and Materials Transactions A. 2016;47(12):6498-506. https://doi.org/10.1007/s11661-016-3730-1

8. Alizadeh M, Safaei H. Characterization of Ni-Cu matrix, Al2O3 reinforced nano-composite coatings prepared by electrodeposition. Applied Surface Science. 2018;456:195-203. https://doi.org/10.1016/j.apsusc.2018.06.095

9. Toghraei M, Siadati H. Electrodeposited co-pi catalyst on α-Fe2O3 photoanode for water-splitting applications. International Journal of Engineering. 2018;31(12):2085-91. 10.5829/ije.2018.31.12c.13

10. KK P. Experimental investigation by cryogenic treatment of aluminium 6063 and 8011 and nicow coating to improve hardness and wear. International Journal of Engineering. 2016;29(6):827-33. https://doi.org/10.5829/idosi.ije.2016.29.06c.12

11. Kumar D, Angra S, Singh S. Mechanical properties and wear behaviour of stir cast aluminum metal matrix composite: a review. International Journal of Engineering. 2022;35(4):794-801. https://doi.org/10.5829/IJE.2022.35.04A.19

12. Moosaei H, Zareei A, Salemi N. Elevated Temperature Performance of Concrete Reinforced with Steel, Glass, and Polypropylene Fibers and Fire-proofed with Coating. International Journal of Engineering. 2022;35(5):917-30. https://doi.org/10.5829/ije.2022.35.05b.08

13. Poursaeidi E, Salarvand A. Comparison of properties of ti/tin/ticn/tialn film deposited by cathodic arc physical vapor and plasma-assisted chemical vapor deposition on custom 450 steel substrates. International Journal of Engineering. 2016;29(10):1459-68. https://doi.org/10.5829/idosi.ije.2016.29.10a.17

14. Allahyarzadeh M, Aliofkhazraei M, Rouhaghdam AS, Torabinejad V. Gradient electrodeposition of Ni-Cu-W (alumina) nanocomposite coating. Materials & Design. 2016;107:74-81. https://doi.org/10.1016/j.matdes.2016.06.019

15. Geramipour F, Khoei SM, Gugtapeh HS. Effect of shaped waveform on structure and electrochemical corrosion behavior of pulse electrodeposited NiCu alloy coatings. Surface and Coatings Technology. 2021;424:127643. https://doi.org/10.1016/j.surfcoat.2021.127643

16. Thurber CR, Ahmad YH, Sanders SF, Al-Shenawa A, D'Souza N, Mohamed AM, et al. Electrodeposition of 70-30 Cu–Ni nanocomposite coatings for enhanced mechanical and corrosion properties. Current Applied Physics. 2016;16(3):387-96. https://doi.org/10.1016/j.cap.2015.12.022

17. Goranova D, Rashkov R, Avdeev G, Tonchev V. Electrodeposition of Ni–Cu alloys at high current densities: details of the elements distribution. Journal of Materials Science. 2016;51:8663-73. https://doi.org/10.1007/s10853-016-0126-y

18. Lee W-H, Chung K. Investigation of a copper–nickel alloy resistor using co-electrodeposition. Journal of Applied Electrochemistry. 2020;50:535-47. https://doi.org/10.1007/s10800-020-01398-0

19. Pingale AD, Belgamwar SU, Rathore JS. Effect of graphene nanoplatelets addition on the mechanical, tribological and corrosion properties of Cu–Ni/Gr nanocomposite coatings by electro-co-deposition method. Transactions of the Indian Institute of Metals. 2020;73:99-107. https://doi.org/10.1007/s12666-019-01807-9

20. Hughes RA, Menumerov E, Neretina S. When lithography meets self-assembly: a review of recent advances in the directed assembly of complex metal nanostructures on planar and textured surfaces. Nanotechnology. 2017;28(28):282002. https://doi.org/10.1088/1361-6528/aa77ce

21. Kamel M, Anwer Z, Abdel-Salam I, Ibrahim I. Electrodeposition of nanocrystalline Ni–Cu alloy from environmentally friendly lactate bath. Surface and Interface Analysis. 2014;46(7):442-8. https://doi.org/10.1002/sia.5525

22. Awasthi S, Pandey SK, Balani K. Tuning the magnetism and tribological behaviour of electrodeposited Ni/Cu bi-layer by selective reinforcement of carbon nanotubes. Journal of Alloys and Compounds. 2020;818:153287. https://doi.org/10.1016/j.jallcom.2019.153287

23. Heidarzadeh A, Saeid T. Correlation between process parameters, grain size and hardness of friction-stir-welded Cu–Zn alloys. Rare Metals. 2018;37:388-98. https://doi.org/10.1007/s12598-016-0704-9

24. Karunakaran M, Pugazhvadivu M, Gunasegaran V, Gowtham G. Electrodeposition of Cu-Ni-PW Composite on Al-6063 Substrate. 2018. https://doi.org/10.26438/ijsrpas/v6i3.5964

25. Karunakaran M, Vadivu MP. Magnetic and micro-mechanical behavior of Cu-Ni-PW-TiO2 hybrid composite electroplating on Al alloy substrate. Journal of Magnetism and Magnetic Materials. 2019;475:359-67. https://doi.org/10.1016/j.jmmm.2018.11.077

26. Soegijono B, Susetyo F, editors. Magnetic field exposure on electroplating process of ferromagnetic nickel ion on copper substrate. Journal of Physics: Conference Series; 2022: IOP Publishing.

27. Deo Y, Guha S, Sarkar K, Mohanta P, Pradhan D, Mondal A. Electrodeposited Ni-Cu alloy coatings on mild steel for enhanced corrosion properties. Applied Surface Science. 2020;515:146078. https://doi.org/10.1016/j.apsusc.2020.146078

28. Seakr R. Microstructure and crystallographic characteristics of nanocrystalline copper prepared from acetate solutions by electrodeposition technique. Transactions of Nonferrous Metals Society of China. 2017;27(6):1423-30. https://doi.org/10.1016/S1003-6326(17)60164-X

29. Dolabella S, Borzì A, Dommann A, Neels A. Lattice strain and defects analysis in nanostructured semiconductor materials and devices by high-resolution X-ray diffraction: theoretical and practical aspects. Small Methods. 2022;6(2):2100932. https://doi.org/10.1002/smtd.202100932

30. Budi S, Tawwabin RA, Cahyana U, Paristiowati M. Saccharin-assisted galvanostatic electrodeposition of nanocrystalline FeCo films on a flexible substrate. International Journal of Electrochemical Science. 2020;15(7):6682-94. https://doi.org/10.20964/2020.07.74

31. Syamsuir S, Soegijono B, Yudanto SD, Basori B, Ajiriyanto MK, Nanto D, et al. Electrolyte Temperature Dependency of Electrodeposited Nickel in Sulfate Solution on the Hardness and Corrosion Behaviors. International Journal of Engineering, Transactions C: Aspects, . 2023;36(6):1193-200. 10.5829/ije.2023.36.06c.18

32. Soegijono B, Susetyo FB, Fajrah MC. Electrodeposition of Paramagnetic Copper Film under Magnetic Field on Paramagnetic Aluminum Alloy Substrates. e-Journal of Surface Science and Nanotechnology. 2020;18:281-8. https://doi.org/10.1380/EJSSNT.2020.281

33. Devi C, Ashokkumar R. INFLUENCE OF DIFFERENT CURRENT DENSITY ON CHARACTERISTICS OF NiFeP NANO ALLOY THIN FILMS. Rasayan Journal of Chemistry. 2018;11(3). https://doi.org/10.31788/RJC.2018.1133088

34. Li B, Mei T, Li D, Du S. Ultrasonic-assisted electrodeposition of Ni-Cu/TiN composite coating from sulphate-citrate bath: Structural and electrochemical properties. Ultrasonics sonochemistry. 2019;58:104680. https://doi.org/10.1016/j.ultsonch.2019.104680

35. Sarac U, Baykul MC. Morphological and microstructural properties of two-phase Ni–Cu films electrodeposited at different electrolyte temperatures. Journal of alloys and compounds. 2013;552:195-201. https://doi.org/10.1016/j.jallcom.2012.10.071

36. Arasteh J. Microhardness Optimization of Al–TiC Nanocomposite Produced by Mechanical Milling and Heat Treatment. Advanced Ceramics Progress. 2021;7(1):35-45. https://doi.org/10.30501/ACP.2021.265197.1052

37. Goranova D, Avdeev G, Rashkov R. Electrodeposition and characterization of Ni–Cu alloys. Surface and Coatings Technology. 2014;240:204-10. https://doi.org/10.1016/j.surfcoat.2013.12.014

38. Hu G, Huang R, Wang H, Zhao Q, Zhang X. Facile galvanic replacement deposition of nickel on copper substrate in deep eutectic solvent and its activation ability for electroless Ni–P plating. Journal of Solid State Electrochemistry. 2022;26(5):1313-22. https://doi.org/10.1007/s10008-022-05172-4

39. Niu J, Song M, Zhang Y, Zhang Z. Dealloying induced nanoporosity evolution of less noble metals in Mg ion batteries. Journal of Magnesium and Alloys. 2021;9(6):2122-32. https://doi.org/10.1016/j.jma.2021.04.003

40. Wang S, Guo X, Yang H, Dai J, Zhu R, Gong J, et al. Electrodeposition mechanism and characterization of Ni–Cu alloy coatings from a eutectic-based ionic liquid. Applied Surface Science. 2014;288:530-6. https://doi.org/10.1016/j.apsusc.2013.10.065

41. Nwaeju CC, Eboh, A. O., and Edoziuno, F. O. . Grain size evolution mechanical and corrosion behaviour of precipitate strengthened Cu-Ni alloy. Acta Metallurgica Slovaca. 2022;28(4):188–96. https://doi.org/10.36547/ams.28.4.1609

42. Ameri Ekhtiarabadi T, Zandrahimi M, Ebrahimifar H. The Impact of Current Density of Electroplating on Microstructure and Mechanical Properties of Ni-ZrO2-TiO2 Composite Coating. Advanced Ceramics Progress. 2020;6(1):22-9. https://doi.org/10.30501/acp.2020.233518.1038

43. Wang C, Hossain Bhuiyan ME, Moreno S, Minary-Jolandan M. Direct-write printing copper–nickel (Cu/Ni) alloy with controlled composition from a single electrolyte using co-electrodeposition. ACS applied materials & interfaces. 2020;12(16):18683-91. https://doi.org/10.1021/acsami.0c01100

44. Hanachi M, Seyedraoufi Z, Abouei V. Investigation of Microstructure, Hardness, and Corrosion Resistance of Ni-P-GO Electroless Nanocomposite Coating on AZ31D Alloy Surface. Advanced Ceramics Progress. 2020;6(3):55-62. https://doi.org/10.30501/acp.2020.233518.1038

45. Dhara B, Jha PK, Gupta K, Bind VK, Ballav N. Diamagnetic Molecules Exhibiting Room-Temperature Ferromagnetism in Supramolecular Aggregates. The Journal of Physical Chemistry C. 2017;121(22):12159-67. https://doi.org/10.1021/acs.jpcc.7b02145

46. Qasim I, Waqee-ur-Rehman M, Mumtaz M, Hussain G, Nadeem K, Shehzad K. Ferromagnetic (Ni) nanoparticles–CuTl-1223 superconductor composites. Journal of Magnetism and Magnetic Materials. 2016;403:60-7. https://doi.org/10.1016/j.jmmm.2015.11.066

47. Padmapriya G, Manikandan A, Krishnasamy V, Jaganathan SK, Antony SA. Enhanced catalytic activity and magnetic properties of spinel Mn x Zn 1− x Fe 2 O 4 (0.0≤ x≤ 1.0) nano-photocatalysts by microwave irradiation route. Journal of Superconductivity and Novel Magnetism. 2016;29:2141-9. https://doi.org/10.1007/s10948-016-3527-x

48. Demidenko O, Zhyvulka A, Yanushkevich K, Galias A, Constantin V, Neacsu E, et al. Magnetic properties of stainless steels under corrosive action of based on choline chloride ionic liquids. Journal of Magnetism and Magnetic Materials. 2019;477:74-6. https://doi.org/10.1016/j.jmmm.2019.01.034

49. Marenych O, Ding D, Pan Z, Kostryzhev A, Li H, van Duin S. Effect of chemical composition on microstructure, strength and wear resistance of wire deposited Ni-Cu alloys. Additive

Manufacturing. 2018;24:30-6. https://doi.org/10.1016/j.addma.2018.08.003

50. Ramkumar KD, Joshi V, Pandit S, Agrawal M, Kumar OS, Periwal S, et al. Investigations on the microstructure and mechanical properties of multi-pass pulsed current gas tungsten arc weldments of Monel 400 and Hastelloy C276. Materials & Design. 2014;64:775-82. https://doi.org/10.1016/j.matdes.2014.08.055

Persian Abstract

چکیده

پوشش‌های آلیاژی تک فاز نیکل مسغنی از نیکل (Ni) بر روی بسترهای آلومینیومی (Al) با رسوب الکتریکی در حمام سیترات تثبیت شده تولید شدند. آزمایش‌های رسوب الکتریکی در چهار چگالی جریان مختلف انجام شد. افزایش چگالی جریان منجر به افزایش سرعت رسوب فلز سریعتر از نرخ تکامل هیدروژن شد. بنابراین، راندمان جریان کاتدی افزایش یافت. سیستم‌های کریستالی آلیاژهای Ni-Cu مکعبی در مرکز سطح (FCC) بودند، با صفحه (۱۱۱) به عنوان صفحه کریستالی ترجیحی. میکروسکوپ الکترونی رویشی با اندازه‌گیری‌های طیف‌سنجی پرتو ایکس پراکنده انرژی (SEM-EDS) نشان داد که محتوای نیکل در پوشش با افزایش چگالی جریان افزایش می‌یابد. نمونه -Ni Cu 40 بیشترین مقدار نیکل را داشت و مورفولوژی همگن و فشرده را نشان داد. مشخص شد که هر چه غلظت نیکل در محلول بیشتر باشد، اندازه دانه کوچکتر است. اندازه‌گیری‌های ثبت‌شده با یک مغناطیس‌سنج نمونه ارتعاشی (VSM) نشان داد که نمونه Ni-Cu 40 اشباع مغناطیسی را ارائه می‌کند، با بالاترین مقدار ۰.۱۰۸. emu/g روش میکروسختی ۴۰۴ HV بر روی نمونه Ni-Cu 40 تولید کرد. در نتیجه، چگالی جریان بالاتر با ترکیب نیکل بالاتر و افزایش ضخامت همراه بود که مسئول افزایش خواص مغناطیسی و سختی بود.

Effect of Current Density on Magnetic and Hardness Properties of Ni-Cu Alloy Coated on Al via Electrodeposition

4   Fatih Doğan, Mehmet Uysal, Erhan Duru, Hatem Akbulut, Serdar Aslan. "Pulsed electrodeposition of Ni-B/TiN composites: effect of current density on the structure, mechanical, tribological, and corrosion properties", Journal of Asian Ceramic Societies, 2020
Publication   1%

5   www.mdpi.com
Internet Source   1%

6   R. SEAKR. "Microstructure and crystallographic characteristics of nanocrystalline copper prepared from acetate solutions by electrodeposition technique", Transactions of Nonferrous Metals Society of China, 2017
Publication   1%

7   Morteza Alizadeh, Hamed Safaei. "Characterization of Ni-Cu matrix, Al 2 O 3 reinforced nano-composite coatings prepared by electrodeposition", Applied Surface Science, 2018
Publication   1%

8   Muthusankar Ganesan, Chao-Chen Liu, Sabarison Pandiyarajan, Chen-Ta Lee, Ho-Chiao Chuang. "Post-supercritical CO2 electrodeposition approach for Ni-Cu alloy fabrication: An innovative eco-friendly
    1%

strategy for high-performance corrosion resistance with durability", Applied Surface Science, 2021
Publication

9   Weiwei Zhang, Wenzhe Xia, Baosong Li, Mingyuan Li, Ming Hong, Zhen Zhang. "Influences of Co and process parameters on structure and corrosion properties of nanocrystalline Ni-W-Co ternary alloy film fabricated by electrodeposition at low current density", Surface and Coatings Technology, 2022
Publication   1%

10   nagaokaut.repo.nii.ac.jp
Internet Source   1%

11   www.scielo.br
Internet Source   1%

12   Begum Unveroglu. "Electrodeposition and Characterization of Ni-Cu Alloy and Submicron-Sized CeO2 Reinforced Ni-Cu Metal Matrix Composite Coatings", Arabian Journal for Science and Engineering, 2022
Publication   <1%

13   Haifeng Tan, Wenchao Yang, Mingzhu Hao, Chao Wang, Jie Yang, Haixuan Sunyu, Yunhe Ling, Guihong Song, Chunlin He. "Effect of Current Density on the Corrosion Resistance and Photocatalytic Properties of Cu-Ni-   <1%

Zn0.96Ni0.02Cu0.02O Nanocomposite Coatings", Materials, 2023
Publication

14 Pengyuan Zhang, Guozhe Meng, Yanqiu Wang, Bing Lei, Fuhui Wang. "Significantly enhanced corrosion resistance of Ni–Cu coating modified by minor cerium", Corrosion Communications, 2021
Publication

<1 %

15 japsonline.com
Internet Source

<1 %

16 M. Karunakaran, M. Pugazh Vadivu. "Magnetic and micro-mechanical behavior of Cu-Ni-P-W-TiO2 hybrid composite electroplating on Al alloy substrate", Journal of Magnetism and Magnetic Materials, 2018
Publication

<1 %

17 Sarac, Umut, and M. Celalettin Baykul. "Morphological and microstructural properties of two-phase Ni–Cu films electrodeposited at different electrolyte temperatures", Journal of Alloys and Compounds, 2013.
Publication

<1 %

18 F. Geramipour, S.M. Mousavi Khoei, H. Shooshtari Gugtapeh. "Effect of shaped waveform on structure and electrochemical corrosion behavior of pulse electrodeposited

<1 %

Ni Cu alloy coatings", Surface and Coatings Technology, 2021
Publication

19 www.acerp.ir   <1%
    Internet Source

20 Kyle D. Gilroy, Aleksey Ruditskiy, Hsin-Chieh   <1%
    Peng, Dong Qin, Younan Xia. "Bimetallic
    Nanocrystals: Syntheses, Properties, and
    Applications", Chemical Reviews, 2016
    Publication

21 Shaohua Wang, Xingwu Guo, Haiyan Yang,   <1%
    JiChun Dai, Rongyu Zhu, Jia Gong, Liming
    Peng, Wenjiang Ding. "Electrodeposition
    mechanism and characterization of Ni–Cu
    alloy coatings from a eutectic-based ionic
    liquid", Applied Surface Science, 2014
    Publication

22 Yuan Yuan, Yuanwei Chen, Jia-Hui Liu, Haifang   <1%
    Wang, Yuanfang Liu. "Biodistribution and fate
    of nanodiamonds in vivo", Diamond and
    Related Materials, 2009
    Publication

23 Submitted to Birla Institute of Technology and   <1%
    Science Pilani
    Student Paper

24 P. Gupta. "Effect of annealing current density   <1%
    on the microstructure of nanocrystalline

FeCuNbSiB alloy", Journal of Applied Physics, 2007
Publication

25   Baosong Li, Tianyong Mei, Dandan Li, Shengsong Du. "Ultrasonic-assisted electrodeposition of Ni-Cu/TiN composite coating from sulphate-citrate bath: Structural and electrochemical properties", Ultrasonics Sonochemistry, 2019   <1%
Publication

26   D. Goranova, R. Rashkov, G. Avdeev, V. Tonchev. "Electrodeposition of Ni–Cu alloys at high current densities: details of the elements distribution", Journal of Materials Science, 2016   <1%
Publication

27   Torabinejad, V., M. Aliofkhazraei, S. Assareh, M.H. Allahyarzadeh, and A. Sabour Rouhaghdam. "Electrodeposition of Ni-Fe alloys, composites, and nano coatings–A review", Journal of Alloys and Compounds, 2017.   <1%
Publication

28   Zuveria Firdouz, Pragya Tripathi, K. Mondal, Kantesh Balani. "Effect of carbonaceous reinforcements on anticorrosive and magnetic properties of Ni Cu based composite coatings prepared by pulsed   <1%

electrodeposition", Surface and Coatings
Technology, 2022
Publication

Exclude quotes   On   Exclude matches   < 15 words
Exclude bibliography   On

Effect of Current Density on Magnetic and Hardness Properties of Ni-Cu Alloy Coated on Al via Electrodeposition